AIP | Journal of Applied Physics

The effect of high-In content capping layers on low-density bimodal-sized InAs quantum dots

G. Trevisi, I. Suárez, L. Seravalli, D. Rivas, P. Frigeri et al.

Citation: J. Appl. Phys. **113**, 194306 (2013); doi: 10.1063/1.4805351
View online: http://dx.doi.org/10.1063/1.4805351
View Table of Contents: http://jap.aip.org/resource/1/JAPIAU/v113/i19
Published by the American Institute of Physics.

JOURNAL OF APPLIED PHYSICS **113**, 194306 (2013)

The effect of high-In content capping layers on low-density bimodal-sized InAs quantum dots

G. Trevisi,[1,a)] I. Suárez,[2] L. Seravalli,[1] D. Rivas,[2] P. Frigeri,[1] G. Muñoz-Matutano,[2] V. Grillo,[1,3] L. Nasi,[1] and J. Martínez-Pastor[2]
[1]*CNR-IMEM Institute, Parco Area delle Scienze 37a, 43124 Parma, Italy*
[2]*UMDO (Unidad Asociada al CSIC-IMM), Instituto de Ciencia de los Materiales, Universidad de Valencia, P.O. Box 22085, 46071 Valencia, Spain*
[3]*CNR-Istituto Nanoscienze S3, Via Campi 213/A, 41125 Modena, Italy*

(Received 8 March 2013; accepted 1 May 2013; published online 16 May 2013)

The structural and morphological features of bimodal-sized InAs/(In)GaAs quantum dots with density in the low $10^9\,cm^{-2}$ range were analyzed with transmission electron microscopy and atomic force microscopy and were related to their optical properties, investigated with photoluminescence and time-resolved photoluminescence. We show that only the family of small quantum dots (QDs) is able to emit narrow photoluminescence peaks characteristic of single-QD spectra; while the behavior of large QDs is attributed to large strain fields that may induce defects affecting their optical properties, decreasing the optical intensity and broadening the homogeneous linewidth. Then, by using a rate-equation model for the exciton recombination dynamics, we show that thermal population of dark states is inhibited in both QD families capped by high In content InGaAs layers. We discuss this behavior in terms of alloy disorder and increased density of point defects in the InGaAs pseudomorphic layer. © *2013 AIP Publishing LLC*. [http://dx.doi.org/10.1063/1.4805351]

I. INTRODUCTION

In recent years, the research on self-assembled semiconductor quantum dots (QDs) led to results of extreme interest from both fundamental and applied points of view; the quantum information field, in particular, has identified III-V semiconductor QDs as practical candidates for the realization of single-photon sources at telecom wavelengths.[1–3] InAs/GaAs structures with a few QDs/μm^2 and emission at 1.3 μm have been successfully prepared by using epitaxial growth conditions that result in large cation migration length[4–6] and by growing pseudomorphic InGaAs upper confining layer (UCL) on top of the QDs.[6,7] A complete picture of QD properties in this type of structures is necessary in order to correctly describe carrier dynamics that strongly depends on peculiar characteristics of the structures such as the energy of excited states and wetting layer (WL),[8] the presence of defects and non-radiative recombination centers[9,10] and also the existence of bimodal QD size distributions.[11] The results of this work, concerning the use of high lattice-mismatched UCL, are of interest also for the realization of structures that employ complex capping layers to engineer the properties of QDs, such as infrared photodetectors[12] and QDs in a well structures.[13,14]

In this work, we present the study of morphological, structural, and optical properties of bimodal-sized InAs QDs deposited by Molecular Beam Epitaxy (MBE) at low growth rate and high growth temperature and capped with InGaAs UCLs.[6] Four samples with different In contents in the barrier ($x = 0$, 0.1, 0.2, and 0.3) were analysed in order to establish the influence of this parameter on the behavior of QDs. To this purpose, the optical properties of the structures were studied by means of photoluminescence (PL), micro-photoluminescence (μPL), and time-resolved PL (TRPL), and were correlated to their structural and morphological properties, investigated with Transmission Electron Microscopy (TEM) and Atomic Force Microscopy (AFM). It has already been shown that the In content in the barrier has a direct influence on the emission properties of QDs, such as the emission energy and the energy barrier for thermal escape of confined carriers.[6,8] In this paper, it is demonstrated that, when the In concentration in pseudomorphic UCLs increases above a certain threshold ($x \geq 0.20$), the exciton dynamics changes in a way that is consistent with the introduction of non-radiative recombination centres in the UCL. In addition, when μPL characterization was performed on the samples, it was possible to discriminate some narrow peaks associated to single QD emission only in the high energy band (corresponding to small QDs). This indicates that the low energy emission is influenced by the presence of defects, which may be related to large strain fields present in large QDs. Such strain-related defects provokes the broadening of the homogeneous linewidth[15] preventing the presence of narrow lines in this range of energies. These results are of particular interest for the realization of single photon emitters at telecom wavelengths based on this sort of QDs.[6,7,16,17]

Finally, a model of carrier dynamics that takes into account the distribution of QD energy levels and the influence of the In content in the UCL is proposed. PL as a function of temperature exhibits two decay channels whose activation energies are correlated to the In content in the barrier alloy. In addition, the simulations explain the observed increase of the recombination time with temperature by considering the participation of dark states in the exciton recombination dynamics.

[a)]Electronic mail: trevisi@imem.cnr.it

II. EXPERIMENTAL

The structures were prepared by MBE on semi-insulating (100)-oriented GaAs substrates: QDs were grown on a 100 nm GaAs buffer deposited at 600 °C and consist of 2.0 ML of InAs grown at 0.01 ML/s at a growth temperature of 520 °C. The QD layer is capped with a 10 nm-thick $In_xGa_{1-x}As$ UCL and a 10 nm-thick GaAs cap layer, both grown by Atomic Layer MBE (ALMBE) at 360 °C. The nominal In content of UCL in different structures is x = 0, 0.1, 0.2, and 0.3. Contact mode AFM measurements were performed on uncapped structures to evaluate the density and morphology of QDs. Scanning TEM (STEM) experiments have been performed using a JEOL 2200FS with SFEG emitter operated at 200 keV. The detection angle has been varied systematically to produce two kinds of detection condition, namely, at low and high angle annular dark field (ADF). The high angle ADF finds a larger application in compositional analysis but this information is somehow mixed with strain effect.[18,19] Here, we use the low angle detection range (LAADF), which is more sensitive to the strain than to the chemical information; the corresponding range is $30 < 2\theta < 84$ mrad. For ensemble QD optical measurements samples were held in a cold finger of a closed-cycle He cryostat, which can be cooled down to 10 K. PL was measured by using a Ti:sapphire mode locked laser at a wavelength of 780 nm. Excitation was fixed to 58 mW/cm^2 and 1.46 W/cm^2 for low and high power conditions, respectively. The μPL experiments were carried out at 4 K using a confocal microscope (Attocube system) to focus the Ti:sapphire laser spot on the sample surface and to collect the μPL signal with a single-mode fiber. In both cases, the signal was dispersed by a double 0.3 m focal length grating spectrograph and detected with a back illuminated InGaAs CCD. TRPL experiments have been carried out with the Ti:sapphire laser in pulsed mode operation (pulse width 2ps and 76 MHz of repetition rate) at the same wavelength. In this case, the emitted signal is collected by an InGaAs avalanche photodiode connected to a time correlated single photon counting electronics. The overall time resolution of the system was estimated to be around 400 ps.

III. EXPERIMENTAL RESULTS

Fig. 1(a) is a top-view AFM micrograph showing the topographical features of uncapped QDs. The estimated surface dot density is 4–5 $\times$ 10^9 cm^{-2}. QD height and diameter distributions were extracted by statistical analysis performed on large area AFM images, by taking into account dot-tip convolution effects to correct the widening of measured base diameter sizes.

The histogram of QD heights in Fig. 1(c), obtained from the analysis of Fig. 1(a), indicates that the QD ensemble exhibits a size distribution: the fitted peak positions, related to the more frequent dot height values, are (6.8 $\pm$ 1.5) nm and (9.5 $\pm$ 1.5) nm, respectively, while comparable mean base diameters of (25.2 $\pm$ 2.5) nm are found for both QD families. The two gaussian curves displayed in Fig. 1(c) have similar relative intensity corresponding to similar density of the two main dot distributions. These results nicely agree with the angle-mapped AFM image displayed in Fig. 1(b), obtained by calculating the surface gradient of height at each point of Fig. 1(a). The grey-scale of Fig. 1(b) is related to the modulus of the surface gradient and shows the local surface slope with respect to the (100)-substrate surface, so that darker regions correspond to steeper facets. This image highlights the existence of at least two QD families that give rise to different contrast, then two different QD morphologies characterized by different slopes of lateral facets should exist.[20,21] Given the high growth temperature and low growth rate used, the observed bimodal distribution of QD size is consistent with the coexistence of different QD shapes explained in the frame of equilibrium energy theories.[22]

Additional information regarding QD size after the complete growth of the structure has been extracted by analysing plan view TEM images: Fig. 2 shows a LAADF image of QDs capped with $In_{0.30}Ga_{0.70}As$ UCL. This technique is suitable to measure the QD diameter, as demonstrated in Ref. 23. By following the approach of Grillo *et al.*[18,19] the LAADF intensity turns out to be proportional to the curvature of the atomic column that, in a QD, is maximum at the QD periphery. The presence of QD compositional gradients, due to In segregation and In-Ga intermixing, could give rise to an ambiguity in the definition of the exact spatial limits of the QD. In such case the region of maximum curvature could be shifted in proximity of the maximum compositional change. However, in the present case, the cross sectional TEM and scanning TEM measurements indicate that most of the compositional change is concentrated in the proximity to the interfaces,[24] that we define as the "metallurgic" interface,

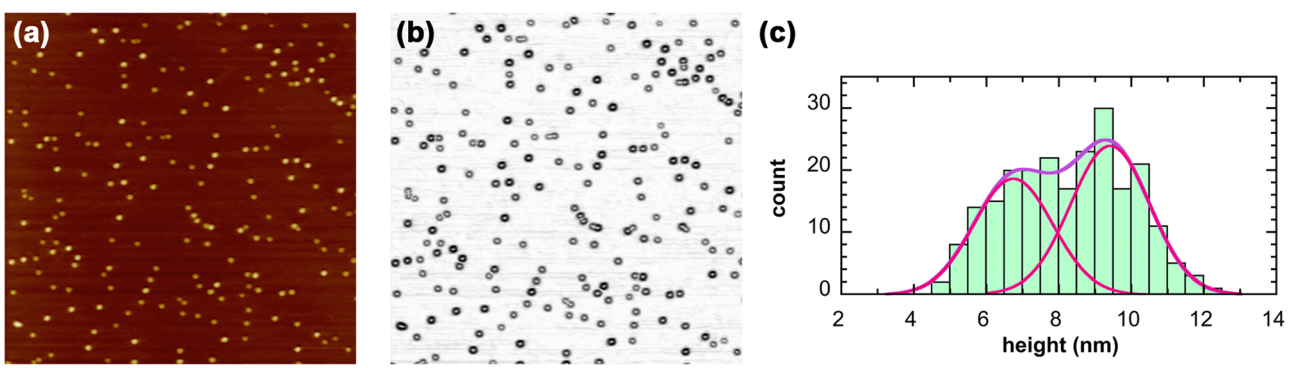

FIG. 1. (a) 2 μm $\times$ 2 μm topographical AFM image, (b) 2 μm $\times$ 2 μm angle-mapped AFM image, in which the gray scale is related to the local surface slope, and (c) histogram of the QD height distribution of uncapped InAs/GaAs QDs.

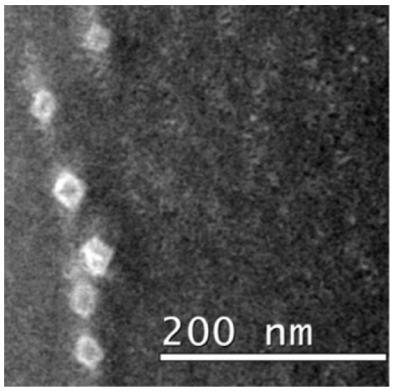

FIG. 2. Experimental LAADF image of InAs QDs capped with $In_{0.30}Ga_{0.70}As$ UCL.

making the above image interpretation more reliable. This observation can be used to estimate with high precision the base diameter of capped QDs, being in the range between 25 and 30 nm.

We note here that these data, obtained with the LAADF technique on capped InAs QDs, are in very good agreement with the estimated QD base-diameter extracted from the AFM images of uncapped QDs. This suggests that the capping procedure, consisting in a low-temperature ALMBE deposition of an (In)GaAs UCL, essentially preserves the QD morphology. The structural characterization revealed also that less than 1% of QDs is relaxed, that is a very small fraction as compared to QD structures grown under similar conditions.[16] On the other hand, we recall here that InGaAs UCLs are not relaxed, also for the higher In content, in accordance with the previous results obtained by X-ray diffraction reciprocal space mapping.[25]

Fig. 3 shows PL spectra of the samples at 13 K; all samples exhibit a bimodal energy distribution that can be deconvoluted into two gaussian curves. They should certainly arise from exciton recombination at the ground states (GS) of two different families of QDs, in agreement with the existence of the bimodal QD height distribution evidenced by AFM measurements (Fig. 1). When increasing the excitation power density, we observe the appearance of additional PL peaks at higher energies than those of the GS (shown in Fig. 3(d) for the $x = 0.30$ structure) that can be attributed to the excited state emission.

The PL peak energies of both QD families shift towards longer wavelengths by increasing the In content in the UCL, thus, leading to the achievement of 1.33 μm emission wavelength at low temperature (T) for the structure with $In_{0.30}Ga_{0.70}As$ UCL.[6] Each PL spectrum of Fig. 3 reveals also a narrow and weaker peak at high energies that can be related to the In(Ga)As WL for the structure with GaAs UCL, or to a combined WL-quantum well (QW) state for the $InAs/In_xGa_{1-x}As$ UCL structures. By increasing the In content, the WL-QW emission energy redshifts from 1.43 to 1.20 eV, while the full width at half maximum (FWHM) is almost constant at 7 meV for $x \leq 0.20$ and then raises up to 11 meV for the structure with $x = 0.30$. In Ref. 25, we studied the structural and optical properties of WLs and QWs of these structures and we showed that, while for low In

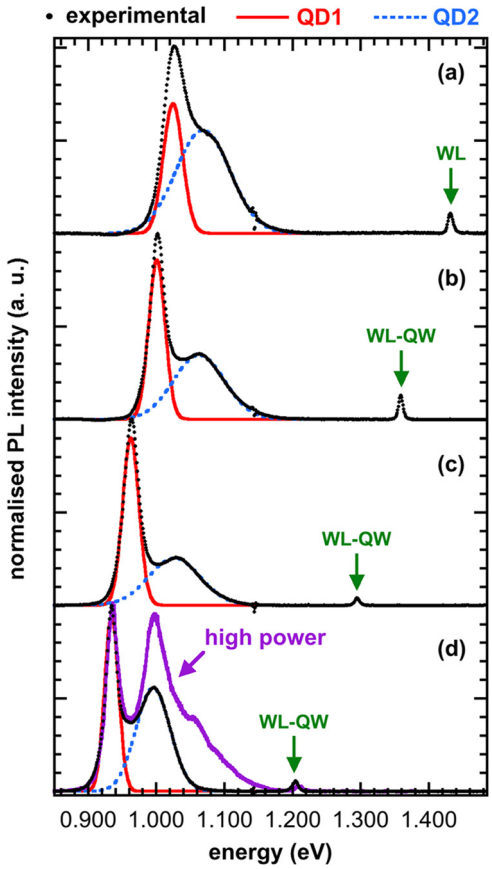

FIG. 3. Normalized PL spectra of QD structures acquired at 13 K under low excitation power density (black dots) and high excitation power density (purple line); the nominal In content in the UCL is: (a) $x = 0$, (b) $x = 0.10$, (c) $x = 0.20$, (d) $x = 0.30$. PL spectra at low excitation power density are fitted with a double-gaussian profile; single gaussian curves labeled as QD1 and QD2 associated to two different QD families are also shown (red continuous lines and blue dashed lines, respectively). The arrows indicate the WL (or WL-QW) emission.

contents, the heavy hole wavefunction is confined close to the lower GaAs/InGaAs interface, for the $x = 0.30$ structure, both the electron and hole wavefunctions are delocalized over the entire UCL. As a consequence, we can infer that the presence of compositionally graded interfaces and alloy disorder in the UCL, which increase with In content,[26] should have a greater influence on the $x = 0.30$ structure than on the other ones. Then, this is a possible explanation for the increase of the WL-QW emission linewidth.

PL emission energies and FWHM of QD families were studied as a function of T in the 10–300 K range, as shown for the structure with nominal $x = 0.20$ in Fig. 4. For all samples, the higher-lying ground state energy level (QD2) is characterized by the so-called "sigmoidal behavior" and the related FWHM ($FWHM_{QD2}$) has a large value at low T (in the 70–110 meV range) that decreases with increasing T. According to the literature,[27–30] this behavior results from the thermally activated transfer of carriers from higher-lying QD energy levels towards lower-lying ones and is typical of QD ensembles characterized by large size distributions. On the other hand, the lower-lying ground state energy level (QD1) does not show such behavior and the related FWHM ($FWHM_{QD1}$) slightly changes with increasing T. These

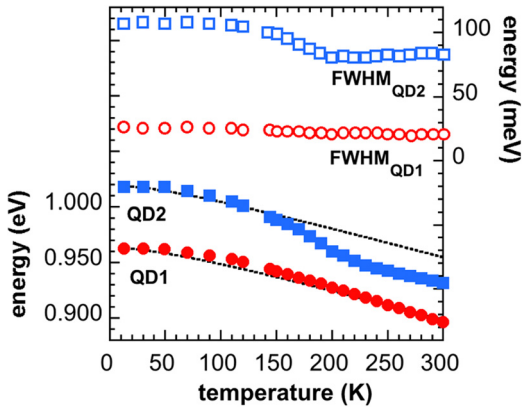

FIG. 4. Peak energies (full symbols) and FWHM (open symbols) of the QD1 and QD2 PL gaussian components as a function of temperature in InAs QDs capped with $In_{0.2}Ga_{0.8}As$ UCL. The Varshni shift of the InAs energy gap (dashed lines) is included for comparison.

observations, together with the fact that all the structures have a $FWHM_{QD1}$ in the 20–30 meV range, suggest that the large-sized QD family has a reduced size dispersion. This may depend on the fact that large-sized QDs are characterized by higher strain fields that, affecting the attachment/detachment of In adatoms to the island edges, favor the so-called size-limiting effect.[31] On the other hand, large strain fields also promote the nucleation of structural defects[32] that could influence the emission properties of QDs.[8] A similar finding can be deduced by the analysis of μPL spectra of the structures. Fig. 5 compares ensemble and μPL spectra of samples with $x = 0.1$ and $x = 0.3$ (the others are similar to the $x = 0.1$ spectrum). Although the QD density is not low enough to see well separated narrow PL lines characteristic of single QD emission, it is possible to distinguish some of them over a background following the high energy PL band. However, the low energy PL band presents similar spectra in ensemble and μPL measurements without narrow peaks, indicating that the family of large-sized QDs can be influenced by the presence of defects or impurities. This can be related to what was observed on very low-density QDs grown on InGaAs metamorphic buffers:[15] while single QDs grown on low-In content buffers exhibited typical narrow exciton peaks, those grown on In-rich layers ($x = 0.30$) exhibited broader single QD excitonic lines. This broadening was attributed to spectral diffusion by impurities or structural defects,[33,34] whose density increases by increasing the In content of the metamorphic buffer.[35]

TRPL for QD1 and QD2 was measured in the four samples as function of T, where recombination times (τ_d) were obtained by fitting the experimental PL transients to single exponential decays, as shown in Fig. 6 for QD1 and QD2 in the sample with $x = 0.30$ at 13 K. Other samples show similar mono-exponential decay curves whose characteristic recombination times will vary with temperature, as described below.

Figs. 7 and 8 show the Arrhenius plot of the integrated PL (a) and recombination time (b) for the two GS bands in the four samples measured under relatively low power excitation conditions. Symbols correspond to experimental data and the red straight lines to the simulation obtained with the model presented below. Given that at low T the integrated PL intensity is constant, data are depicted from 50 K to 300 K in order to better illustrate exciton decay at intermediate and high T. In all cases, the integrated PL presents the same behavior with three different regions: a low T region where the intensity is approximately constant (13–90 K), a weak decrease at middle T (90–210 K), and a sharp decrease at high T (220–300 K). This sharp PL quenching starts at relatively high T (about 220 K) in all the structures, suggesting that InGaAs UCLs provide good carrier confinement even at high In content. The observed Arrhenius dependence would be accounted for by two activation energies, as commonly observed in similar QD structures.[26,36–39] The sharp decrease of the PL intensity corresponds to a large activation energy (200–400 meV) that depends on the barrier composition (see Tables I and II); the energy difference is consistent with the thermionic electron-hole escape from QD to the WL/WL-QW (for UCL structures).

The smooth decrease of the integrated PL intensity at intermediate T can be fitted with a smaller activation energy

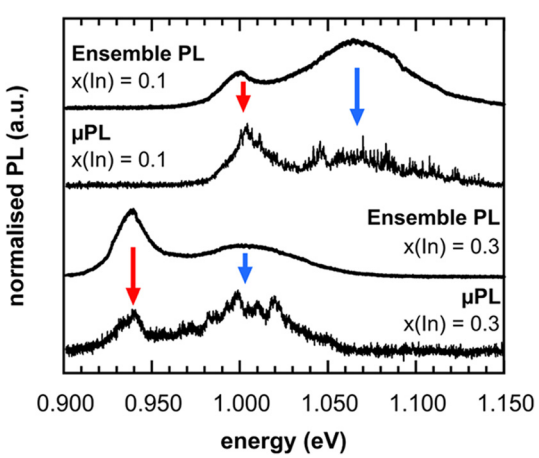

FIG. 5. Ensemble and μPL characterization of samples with $x = 0.3$ and $x = 0.1$. Red and blue arrows indicate QD1 and QD2 peak energies, respectively.

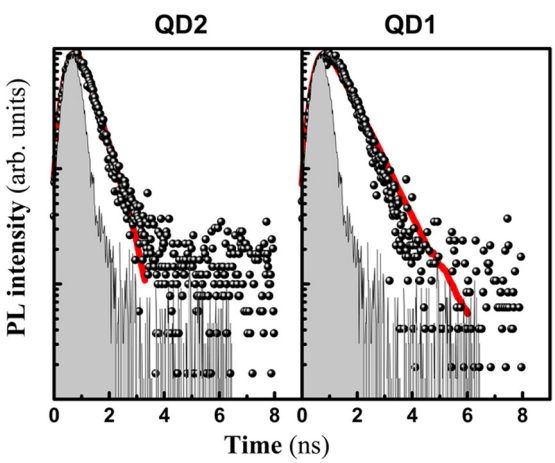

FIG. 6. PL decay curves (dot symbols) at 13 K for QD1 and QD2 families in the $x = 0.30$ sample. The red straight line corresponds to a monoexponential fit by taking into account the temporal response of the system, as obtained by measuring the laser pulses through the experimental setup (grey-shaded transients).

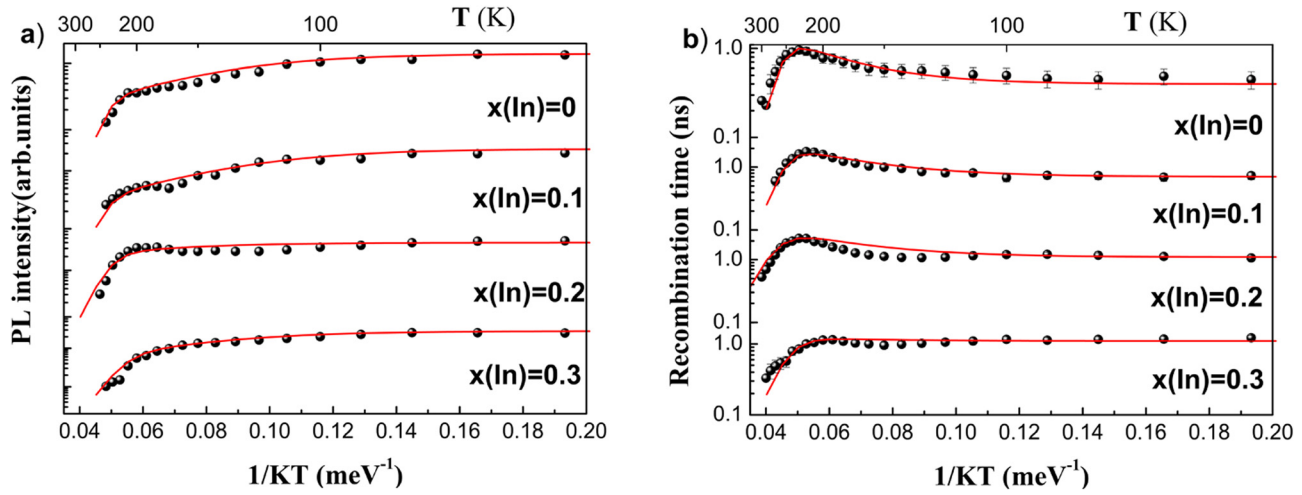

FIG. 7. Arrhenius plots of the integrated PL (a) and the recombination time (b) of the fundamental state QD1 in the four samples. Symbols correspond to the experimental data and straight lines to the simulation.

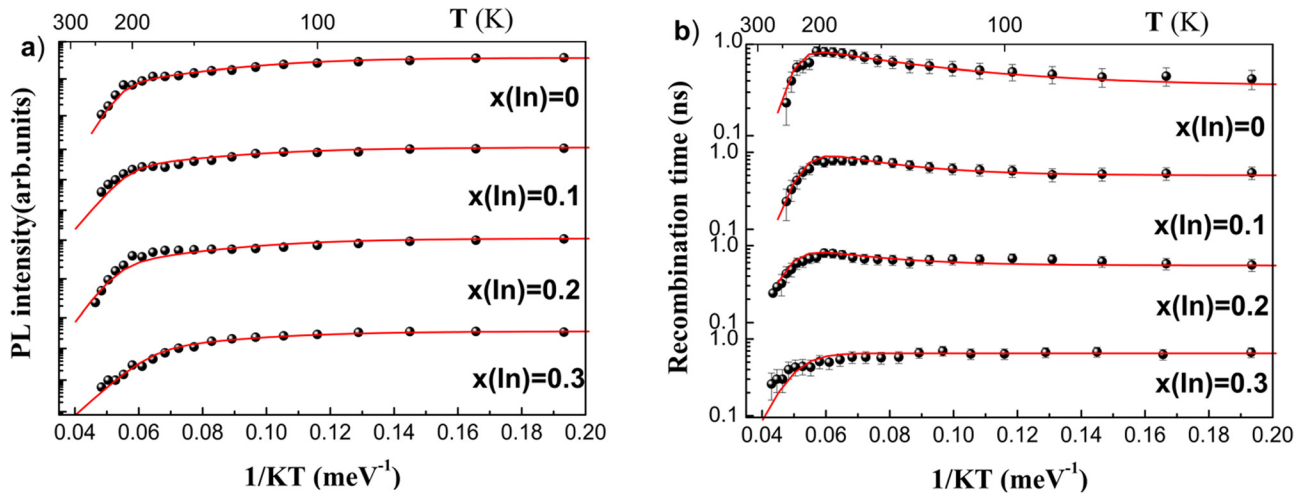

FIG. 8. Arrhenius plots of the integrated PL (a) and the recombination time (b) of the fundamental state QD2 in the four samples. Symbols correspond to the experimental data and straight lines to the simulation.

(20–80 meV) that does not depend critically on the barrier composition. This behavior has been already observed in similar structures and it has been justified by different hypotheses including resonant energy levels between different families,[40] losses of carriers from the WL to the GaAs,[26,36] losses within the barrier itself,[38,39] or losses related to defects.[8,11,37] With the exception of the structure with x = 0.30, three regions can be distinguished in the temperature variation of the recombination time in all samples for QD1 (Fig. 7(b)) and QD2 (Fig. 8(b)) families:

(i) Low-T range (13–50 K, where the PL decay time is practically constant and hence mainly radiative (thermionic losses should be considered negligible).
(ii) Mid-T range (50–220 K), where an increase of τ_d is observed until reaching a maximum value at around 200–220 K, whose origin will be discussed below.
(iii) High-T range (220–300 K), where the observed decrease of τ_d is attributed to thermionic losses.[28]

The observed increase in τ_d in the mid-T range is characterized by an activation energy between 20 and 80 meV, as

TABLE I. QD1 fitting parameters.

	E_a (meV)		Integrated PL			TRPL		
Sample	E_{a1}	E_{a2}	A	a_1	a_2	τ_d (ns)	a_3	g_2
In = 0	395	40	1.4×10^4	7.2×10^8	25	0.4	9×10^6	10
In = 0.1	355	40	2.2×10^4	1.4×10^8	38	0.7	1.4×10^7	13
In = 0.2	330	40	4×10^4	2.2×10^7	5	1.1	1×10^5	10
In = 0.3	270	40	2.8×10^4	8×10^6	24	1.1	3×10^5	1

TABLE II. QD2 fitting parameters.

	E_a (meV)		Integrated PL			TRPL		
Sample	E_{a1}	E_{a2}	A	a_1	a_2	τ_d (ns)	a_3	g_2
In = 0	339	40	2×10^4	5×10^8	35	0.35	5×10^6	15
In = 0.1	288	40	11.6×10^4	5×10^7	30	0.5	1×10^6	9
In = 0.2	265	40	12×10^4	5.5×10^6	27.5	0.55	1×10^5	5
In = 0.3	210	40	4×10^4	2×10^6	30	0.65	3×10^4	0.1

in other similar nanostructures,[41,42] InAs/GaAs self-assembled QDs[43,44] and quantum ring nanostructures.[45,46] The origin of this behavior has been attributed to a thermally induced population of dark excitons;[44,45] where transitions p_e-s_e (or p_h-s_h), initially forbidden, becomes allowed due to thermal transfer.[47] Comparing the Arrhenius plots for PL intensity and τ_d in each sample, one can observe that the main PL quenching mechanism starts at the same mid-T range and very close activation energies are deduced for each UCL composition. Moreover, the fact that both QD1 and QD2 families exhibit the same behavior (Figs. 7 and 8) suggests that the same mechanism would apply in both families.

IV. MODEL FOR EXCITON RECOMBINATION DYNAMICS

In order to give support of our qualitative interpretation of the results in the last section, we propose here a recombination kinetic model depicted in Fig. 9. As it has been proposed in Ref. 28, excitons are photogenerated in the WL at a rate G, where they can recombine with a time constant τ_{WL} (effective decay time accounting for radiative and non-radiative processes) or they can be captured into QDs with a time constant τ_{QD}. Excitons confined in the QDs can recombine radiatively with the time constant τ_d (associated to the experimental recombination time) or can be activated by thermionic emission to the WL states, a mechanism represented by the time τ^*_{QD}. These assumptions are usually considered to model carrier dynamics and thermal escape in InAs/GaAs self assembled QDs,[28] annealed InAs/GaAs QDs,[36] QDs in a barrier.[26] Finally, it is possible to represent the exchange of carriers between the GS and the dark state (DS) by the time constants τ^*_O and τ_O, respectively, including the eventual thermionic emission from the DS to the WL through the time τ_{DS}.[45] Therefore, the exciton recombination dynamics in our QDs can be described by the following coupled rate equations:

$$\frac{dN_{WL}}{dt} = -\frac{N_{WL}}{\tau_{WL}} - \frac{N_{WL}}{\tau_{QD}} + \frac{N_{QD}}{\tau^*_{QD}} + \frac{N_{DS}}{\tau_{DS}} + G, \tag{1}$$

$$\frac{dN_{DS}}{dt} = -\frac{N_{DS}}{\tau_{DS}} - \frac{N_{DS}}{\tau_O} + \frac{N_{QD}}{\tau^*_O}, \tag{2}$$

$$\frac{dN_{QD}}{dt} = -\frac{N_{QD}}{\tau_R} - \frac{N_{QD}}{\tau^*_{QD}} - \frac{N_{QD}}{\tau^*_O} + \frac{N_{DS}}{\tau_O} + \frac{N_{WL}}{\tau_{QD}}, \tag{3}$$

where N_{WL}, N_{DS}, and N_{QD} are exciton populations at the wetting layer, dark state, and quantum dot ground state, respectively. The time constants marked by "*" are related to capture times (τ_{QD} and τ_O) multiplied by the corresponding Maxwell-Boltzmann thermal factor[45]

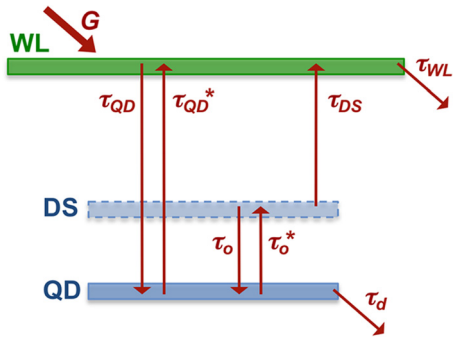

FIG. 9. State diagram proposed to interpret the observed exciton recombination dynamics. Different processes involving the capture, excitation and recombination of carriers in the WL, DS, and GS of QD are indicated by red arrows.

$$\tau^*_{QD} = \frac{\tau_{QD}}{g_1}\exp\left(E_{WL-QD}/KT\right), \tag{4}$$

$$\tau^*_O = \frac{\tau_O}{g_2}\exp\left(E_{DS-QD}/KT\right), \tag{5}$$

where g_1 and g_2 are constants related to the degeneracy of GS and DS, respectively, and E_{WL-QD} and E_{DS-QD} are defined as the activation energies between the quantum dot GS and the wetting layer and between the GS and the DS. Using Eqs. (3)–(5) in steady state conditions, the integrated PL intensity is found to be

$$I = G\frac{\tau_{QD}^{-1}}{\tau_{QD}^{-1}+\tau_{WL}^{-1}}\left[1+\frac{\tau_{QD}^{-1}}{\tau_d^{-1}}\frac{g_1}{\tau_{QD}^{-1}+\tau_{WL}^{-1}}\exp\left(-E_{WL-QD}/KT\right)\right.$$
$$\left.+\frac{\tau_O^{-1}}{\tau_d^{-1}}\frac{g_2}{\tau_{DS}^{-1}+\tau_O^{-1}}\frac{\tau_{WL}^{-1}}{\tau_{QD}^{-1}+\tau_{WL}^{-1}}\exp\left(-E_{DS-QD}/KT\right)\right]^{-1}. \tag{6}$$

This equation can be written in the form:

$$I = \frac{A}{1+a_1\exp\left(-E_{WL-QD}/KT\right)+a_2\exp\left(-E_{DS-QD}/KT\right)}, \tag{7}$$

where A, a_1, and a_2 are fitting constants, and E_{WL-QD} and E_{DS-QD} are the activation energies corresponding to losses from the GS to the WL and DS.

Following the approximation proposed in Ref. 45, if N_{WL} is neglected and one assumes N_{QD} proportional to $\exp(-t/\tau_d)$, the effective PL decay time can be written as

$$\tau_d = \frac{\tau_d(13\text{K})\left[1+g_2\exp\left(-E_{DS-QD}/KT\right)\right]}{1+\tau_d(13\text{K})\left[\frac{g_1}{\tau_{QD}}\exp\left(-E_{WL-QD}/KT\right)+\frac{g_2}{\tau_{DS}}\exp\left(-E_{DS-QD}/KT\right)\right]}. \tag{8}$$

Given that the PL decay time contains radiative and non radiative contributions[44]

$$\frac{1}{\tau_d} = \frac{1}{\tau_R} + \frac{1}{\tau_{NR}}, \tag{9}$$

where τ_R corresponds to the radiative time, approximately equal to the measured value $\tau_d(13\,K)$, and τ_{NR} to the non-radiative time (mainly determined by the thermionic emission of carriers towards the WL)

$$\tau_R = \tau_d(13\mathrm{K})\left[1 + g_2 \exp\left(-E_{DS-QD}/KT\right)\right], \quad (10)$$

$$\tau_{NR} = \frac{\left[1 + g_2 \exp\left(-E_{DS-QD}/KT\right)\right]}{\left[\frac{g_1}{\tau_{QD}} \exp\left(-E_{WL-QD}/KT\right) + \frac{g_2}{\tau_{DS}} \exp\left(-E_{DS-QD}/KT\right)\right]}. \quad (11)$$

According to Eq. (10), the presence of dark states causes an increase of τ_R when T increases with an activation energy equal to the difference between the ground and dark states. In principle, one can assume that τ_{DS} is very long as compared to the other time constants and the effective PL decay time can be approximated by

$$\tau_d = \frac{\tau_d(13\mathrm{K})\left[1 + g_2 \exp\left(-E_{DS-QD}/KT\right)\right]}{1 + \tau_d(13\mathrm{K})\frac{g_1}{\tau_{QD}} \exp\left(-E_{WL-QD}/KT\right)}. \quad (12)$$

The two activation energies appearing in Eqs. (7) and (12) should be consistent with the experimental T dependence found for both the integrated PL intensity and the exciton recombination time shown in Figs. 7 and 8, where continuous lines stand for the best fits. It is interesting to point out that the model works for the four samples in both the PL and the TRPL simulations. The first activation energy is related to the main carrier loss mechanism in QDs, the thermionic emission of carriers towards the WL, and it has been fixed to the value measured by PL spectroscopy (Fig. 3) of the energy difference between the two states ($E_{a1} = E_{WL} - E_{QD}$) in each sample. The second activation energy is related to the DS and is used as a fitting parameter. This energy can oscillate between 20 and 80 meV and a value of 40 ± 10 meV has been chosen for fitting/simulating curves in Figs. 7 and 8. The difference between the p_e-p_h and s_e-s_h optical transitions in the PL spectrum was around 70 meV. Thus, taking in account that separation in electron states is higher than in hole ones, the dark exciton, corresponding to the energy separation p_e-s_e (or p_h-s_h),[45] should be higher than half of this value, and hence 40 meV is a reasonable value for the energy difference. Tables I and II summarize the fitting parameters, were a_3 is given by

$$a_3 \approx \frac{\tau_d(13\mathrm{K})}{\tau_{QD}} g_1. \quad (13)$$

The weights a_1 and a_3 have the same order of magnitude (in general, $\sim 10^5$–10^6) and are related to the thermionic electron-hole escape from QD to the WL. The weights a_2 and g_2 have the same order of magnitude (~ 10) as well and are related to the first activation energy in the PL and to the increase of the recombination time. The second one seems to decrease with the indium composition in the UCL.

The agreement is reasonable in samples with low indium content (x = 0–0.1), where a clear increase of τ_d is observed. In samples with high In content (0.2–0.3), a more complicate (sigmoidal) behavior is observed for τ_d in the same T region of interest (below 200 K). A similar dependence has been found in Ref. 44 for InAs/GaAs QDs grown in p-doped samples; in this case, the behavior was attributed to holes escaping from charged QDs. In our case, since both QD1 and QD2 families exhibit this behavior, we can conclude that it does not depend on peculiar features of QDs but it should rather depend on the characteristics of the high In content UCL. The dependence shown in Figs. 7 and 8 for samples with high In content could be attributed to the presence of non-radiative recombination centers related to compositionally graded interfaces and alloy disorder in the high In-content InGaAs UCL.[38] Recently, it has been shown that the formation energy of point defects such as As vacancies into $In_xGa_{1-x}As$ alloys strongly depends on x, and is almost maximum when x is larger than 0.25.[48] This observation is in agreement with the linewidth increase of the WL-QW emission observed for the x = 0.30 structure.

V. CONCLUSIONS

QD structures of interest for the realization of single photon sources emitting at telecom wavelengths were prepared by MBE, consisting in InAs QDs capped by In(Ga)As pseudomorphic UCLs with different In contents. All the structures showed the presence of bimodal-sized QDs that give rise to the observed double-PL band spectra. The μPL experiments only showed narrow peaks characteristic of single QD emission (homogeneously broadened) for the high-energy emitting QD family (QD2). This observation can be connected to the fact that large QDs are subjected to the presence of high strain fields and that their emission may be affected by the presence of defects associated to them that can broaden the excitonic optical transitions; in fact, independently of x, a small fraction of QDs are relaxed. Both QD families exhibited the same PL temperature dependence, with a fast and a slow decay mechanism; the first one has been related to the escape of carriers from the QDs to the WL-QW energy level, and the second one has been attributed to the presence of DS, as suggested by TRPL characterization. In order to interpret the observed exciton recombination dynamics, we developed a rate-equation model that takes into account the thermal population of dark states; the model well described the observed PL and TRPL behaviors in nanostructures with In content $x < 0.20$, while the high In content structures ($x = 0.30$) showed a more complex τ_d thermal dependence. This suggested that the increase of In content above the x = 0.20 threshold in the UCL may lead to the formation of non-radiative recombination centers that hinders the relaxation mechanism through the dark state population, even when plastic relaxation of the UCL is not reached.

These results will be very valuable for the advanced design of single photon sources based on InAs/InGaAs QD structures that can emit in the 1.3 μm telecom window.

ACKNOWLEDGMENTS

This work was supported through the Spanish MCINN and Generalitat Valenciana Grants Nos. TEC2011-29120-

C05-01 and PROMETEO/2009/074, respectively, and by the 'SANDiE' Network of Excellence of EC, Contract No. NMP4-CT-2004-500101. AFM measurements were carried out at CIM-Parma University.

[1]C. L. Salter, R. M. Stevenson, I. Farrer, C. A. Nicoll, D. A. Ritchie, and A. J. Shields, Nature **465**, 594 (2010).
[2]A. Faraon, A. Majumdar, D. Englund, E. Kim, M. Bajcsy, and J. Vuckovic, New J. Phys. **13**, 055025 (2011).
[3]T. B. Hoang, J. Beetz, L. Midolo, M. Skacel, M. Lermer, M. Kamp, S. Hofling, L. Balet, N. Chauvin, and A. Fiore, Appl. Phys. Lett. **100**, 061122 (2012).
[4]P. B. Joyce, T. J. Krzyzewski, G. R. Bell, T. S. Jones, S. Malik, D. Childs, and R. Murray, Phys. Rev. B **62**, 10891 (2000).
[5]S. Huang, Z. Niu, H. Ni, Y. Xiong, F. Zhan, Z. Fang, and J. Xia, J. Cryst. Growth **301–302**, 751 (2007).
[6]G. Trevisi, L. Seravalli, P. Frigeri, and S. Franchi, Nanotechnology **20**, 415607 (2009).
[7]B. Alloing, C. Zinoni, V. Zwiller, L. H. Li, C. Monat, M. Gobet, G. Buchs, A. Fiore, E. Pelucchi, and E. Kapon, Appl. Phys. Lett. **86**, 101908 (2005).
[8]L. Seravalli, G. Trevisi, P. Frigeri, S. Franchi, M. Geddo, and G. Guizzetti, Nanotechnology **20**, 275703 (2009).
[9]T. V. Torchynska, J. Appl. Phys. **104**, 074315 (2008).
[10]T. E. Nee, Y. F. Wu, C. C. Cheng, and H. T. Shen, J. Appl. Phys. **99**, 013506 (2006).
[11]G. Muñoz-Matutano, I. Suárez, J. Canet-Ferrer, B. Alén, D. Rivas, L. Seravalli, G. Trevisi, P. Frigeri, and J. Martínez-Pastor, J. Appl. Phys. **111**, 123522 (2012).
[12]S. Adhikary, Y. Aytac, S. Meesala, S. Wolde, A. G. U. Perera, and S. Chakrabarti, Appl. Phys. Lett. **101**, 261114 (2012).
[13]S. Krishna, S. Raghavan, G. von Winckel, A. Stintz, G. Ariyawansa, S. G. Matsik, and A. G. U. Perera, Appl. Phys. Lett. **83**, 2745 (2003).
[14]H. Y. Liu, M. Hopkinson, C. N. Harrison, M. J. Steer, R. Frith, I. R. Sellers, D. J. Mowbray, and M. S. Skolnick, J. Appl. Phys. **93**, 2931 (2003).
[15]L. Seravalli, G. Trevisi, P. Frigeri, D. Rivas, G. Muñoz-Matutano, I. Suárez, B. Alén, J. Canet-Ferrer, and J. P. Martínez-Pastor, Appl. Phys. Lett. **98**, 173112 (2011).
[16]B. Alloing, C. Zinoni, L. H. Li, A. Fiore, and G. Patriarche, J. Appl. Phys. **101**, 024918 (2007).
[17]L. Seravalli, G. Trevisi, and P. Frigeri, Cryst. Eng. Comm. **14**, 6833 (2012).
[18]V. Grillo and F. Rossi, J. Cryst. Growth **318**, 1151 (2011).
[19]V. Grillo, K. Mueller, K. Volz, F. Glas, T. Grieb, and A. Rosenauer, J. Phys.: Conf. Ser. **326**, 012006 (2011).
[20]M. A. Lutz, R. M. Feenstra, P. M. Mooney, J. Tersoff, and J. O. Chu, Surf. Sci. Lett. **316**, L1075 (1994).
[21]T. I. Kamins, G. Medeiros-Ribeiro, D. A. A. Ohlberg, and R. S. Williams, J. Appl. Phys. **85**, 1159 (1999).
[22]P. Kratzer, Q. K. K. Liu, P. Acosta-Diaz, C. Manzano, G. Costantini, R. Songmuang, A. Rastelli, O. G. Schmidt, and K. Kern, Phys. Rev. B **73**, 205347 (2006).
[23]V. Grillo and E. Rotunno, Ultramicroscopy **125**, 97 (2013).
[24]G. Trevisi, L. Seravalli, P. Frigeri, C. Bocchi, V. Grillo, L. Nasi, I. Suárez, D. Rivas, G. Muñoz-Matutano, and J. Martínez-Pastor, Cryst. Res. Technol. **46**, 801 (2011).
[25]L. Seravalli, C. Bocchi, G. Trevisi, and P. Frigeri, J. Appl. Phys. **108**, 114313 (2010).
[26]T. V. Torchynska, J. L. Casas Espinola, L. V. Borkovska, S. Ostapenko, M. Dybiec, O. Polupan, N. O. Korkunska, A. Stintz, P. G. Eliseev, and K. J. Malloy, J. Appl. Phys. **101**, 024323 (2007).
[27]L. Brusaferri, S. Sanguinetti, E. Grilli, M. Guzzi, A. Bignazzi, F. Bogani, L. Carraresi, M. Colocci, A. Bosacchi, P. Frigeri, and S. Franchi, Appl. Phys. Lett. **69**, 3354 (1996).
[28]S. Sanguinetti, M. Henini, M. Grassi Alessi, M. Capizzi, P. Frigeri, and S. Franchi, Phys. Rev. B **60**, 8276 (1999).
[29]P. Dawson, O. Rubel, S. D. Baranovskii, K. Pierz, P. Thomas, and E. O. Göbel, Phys. Rev. B **72**, 235301 (2005).
[30]M. B. Smirnov, V. G. Talalaev, B. V. Novikov, S. V. Sarangov, N. D. Zakharov, P. Werner, U. Gösele, J. W. Tomm, and G. E. Cirlin, Phys. Status Solidi B **247**, 347 (2010).
[31]N. P. Kobayashi, T. R. Ramachandran, P. Chen, and A. Madhukar, Appl. Phys. Lett. **68**, 3299 (1996).
[32]D. L. Sales, J. Pizarro, P. L. Galindo, R. Garcia, G. Trevisi, P. Frigeri, L. Nasi, S. Franchi, and S. I. Molina, Nanotechnology **18**, 475503 (2007).
[33]M. Abbarchi, F. Troiani, C. Mastrandrea, G. Goldoni, T. Kuroda, T. Mano, K. Sakoda, N. Koguchi, S. Sanguinetti, A. Vinattieri, and M. Gurioli, Appl. Phys. Lett. **93**, 162101 (2008).
[34]P. Alonso-González, B. Alén, D. Fuster, Y. González, L. González, and J. Martínez-Pastor, Appl. Phys. Lett. **91**, 163104 (2007).
[35]L. Seravalli, P. Frigeri, L. Nasi, G. Trevisi, and C. Bocchi, J. Appl. Phys. **108**, 064324 (2010).
[36]E. C. Le Ru, J. Fack, and R. Murray, Phys. Rev. B **67**, 245318 (2003).
[37]S. Mazzucato, D. Nardin, M. Capizzi, A. Polimeni, A. Frova, L. Seravalli, and S. Franchi, Mater. Sci. Eng., C **25**, 830 (2005).
[38]D. P. Popescu, P. G. Eliseev, A. Stintz, and K. J. Malloy, Semicond. Sci. Technol. **19**, 33 (2004).
[39]D. Colombo, S. Sanguinetti, E. Grilli, M. Guzzi, L. Martinelli, M. Gurioli, P. Frigeri, G. Trevisi, and S. Franchi, J. Appl. Phys. **94**, 6513 (2003).
[40]W. Ouerghui, J. Martínez-Pastor, J. Gomis, A. Melliti, M. A. Maaref, D. Granados, and J. M. García, Eur. Phys. J.: Appl. Phys. **35**, 159 (2006).
[41]L. Kong, Z. Wu, Z. C. Feng, and I. T. Ferguson, J. Appl. Phys. **101**, 126101 (2007).
[42]L. Kong, Z. C. Feng, Z. Wu, and W. Lu, J. Appl. Phys. **106**, 013512 (2009).
[43]M. Gurioli, A. Vinattieri, M. Zamfirescu, M. Colocci, S. Sanguinetti, and R. Nötzel, Phys. Rev. B **73**, 085302 (2006).
[44]E. Harbord, P. Spencer, E. Clarke, and R. Murray, Phys. Rev. B **80**, 195312 (2009).
[45]J. Gomis, J. Martínez-Pastor, B. Alén, D. Granados, J. M. García, and P. Roussignol, Eur. Phys. J. B **54**, 471 (2006).
[46]C. H. Lin, H. S. Lin, C. C. Huang, S. K. Su, S. D. Lin, K. W. Sun, C. P. Lee, Y. K. Liu, M. D. Yang, and J. L. Shen, Appl. Phys. Lett. **94**, 183101 (2009).
[47]B. Yang, J. E. Schneeloch, Z. Pan, M. Furis, and M. Achermann, Phys. Rev. B **81**, 073401 (2010).
[48]S. T. Murphy, A. Chroneos, R. W. Grimes, C. Jiang, and U. Schwingenschlögl, Phys. Rev. B **84**, 184108 (2011).